JOURNAL OF GEOPHYSICAL RESEARCH, VOL. 107, NO. D20, 8038, 10.1029/2000JD000306, 2002

Comparison of inundation patterns among major South American floodplains

Stephen K. Hamilton,[1] Suzanne J. Sippel,[1,2] and John M. Melack[2]

Received 27 December 2000; revised 18 July 2001; accepted 19 October 2001; published 22 August 2002.

[1] A comparative view of inundation patterns in the large floodplains of South America was derived by analysis of the 37-GHz polarization difference observed by the Scanning Multichannel Microwave Radiometer (SMMR; Nimbus-7 satellite, 1979–1987). The following floodplains were analyzed: (1) mainstem Amazon River floodplain in Brazil; (2) Llanos de Moxos (Beni and Mamoré rivers) in Bolivia; (3) Bananal Island (Araguaía River) in Brazil; (4) Llanos del Orinoco (Apure and Meta rivers) in Venezuela and Colombia; (5) Roraima savannas (Branco and Rupununi rivers) in Brazil and Guyana; and (6) Pantanal wetland (Paraguay River) in Brazil. The maximum areas subject to inundation in each region, which include permanent open waters of river channels and lakes, were as follows (in km^2): mainstem Amazon 97,360, Moxos 92,094, Bananal 58,550, Orinoco 107,530, Roraima 16,530, and Pantanal 130,920. The duration of inundation was correlated with the maximum area inundated. Predictive relationships between flooded area and water levels in the nearby rivers allowed extension of the inundation record over nearly a century for the Amazon and Pantanal and several decades for the other floodplains. Interannual variability in the maximum extent of inundation is greatest in the Pantanal, followed by Roraima and Bananal. Based on these extended records, the long-term mean inundation areas (in km^2 and including rivers and lakes) were as follows: mainstem Amazon 46,920, Moxos 29,460, Bananal 13,110, Orinoco 34,700, Roraima 3,480, and Pantanal 34,880. This information is fundamental for hydrological, biogeochemical, and ecological studies of these floodplain-river systems and will improve estimates of methane and other trace gas emissions to the atmosphere from these vast wetlands. *INDEX TERMS:* 1821 Hydrology: Floods; 1860 Hydrology: Runoff and streamflow; 1890 Hydrology: Wetlands; *KEYWORDS:* South America, floodplains, rivers, hydrology, inundation

1. Introduction

[2] Extensive floodplains are associated with the large rivers in South America, and in contrast to the more populated regions of the world, most of these floodplains retain their natural hydrological characteristics. Inundation of floodplains along the larger rivers tends to occur as a single annual flood pulse that lasts for months [*Junk et al.*, 1989]. Where floodplains are a significant component of the fluvial system, they can alter the transport of water and dissolved and particulate materials from upland watersheds through river systems to the sea. Water from riverine overflow or local precipitation and runoff that passes through floodplains is delayed in its transit through the fluvial system, increasing losses by evapotranspiration. During residence in floodplains, floodwaters frequently undergo substantial biogeochemical modifications under the influence of processes such as sedimentation, nutrient uptake by the biota, and changes in redox conditions [*Lewis and Saunders*, 1989; *Richey et al.*, 1989; *Mertes et al.*, 1996; *Hamilton et al.*, 1997].

[3] The maximum extent of floodplain inundation, even if attained only occasionally, delineates the floodplain ecosystem because occasional floods shape the geomorphology [*Mertes et al.*, 1996], exert control over the plant and animal life [*Junk et al.*, 1989], and impact human occupation and land use [*Junk et al.*, 2000]. The productivity of fisheries in tropical rivers is correlated with the extent of seasonal floodplain inundation [*Welcomme*, 1985]. Ecologists are interested in the seasonal timing, predictability, and interannual variability in the flood pulse because those features affect the ability of the biota to cope with and benefit from the inundation, and thereby influence which plants and animals can inhabit a particular floodplain.

[4] The degree of seasonal desiccation of a floodplain during the dry season determines the amount of refuge that persists for aquatic life as well as the expansion of terrestrial habitat, although in some cases the desiccation is sufficiently severe that soil moisture or periodic burning becomes limiting for terrestrial plant growth. Floodplains that alternate seasonally between inundation and desiccation, with both conditions presenting stresses that limit the plant life, have been referred to as "hyperseasonal" eco-

[1]W. K. Kellogg Biological Station and Department of Zoology, Michigan State University, Hickory Corners, Michigan, USA.

[2]Institute for Computational Earth System Science and Department of Ecology, Evolution, and Marine Biology, University of California, Santa Barbara, California, USA.

0148-0227/02/2000JD000306$09.00

systems [*Sarmiento*, 1983]. Savanna floodplains throughout the tropics are important as grazing lands for cattle, and although the seasonal flooding can be an impediment to ranching, the role of flooding in enhancing the production of native pastures and alleviating dry-season stresses is generally recognized [e.g., *Wilcox*, 1992]. The floodplains with the greatest time lags between rainfall and inundation tend to have less desiccation stress for the plant life during the local dry season.

[5] The Large Scale Biosphere-Atmosphere Experiment in Amazônia (LBA), an international research initiative led by Brazil, is designed to improve understanding of the physical, chemical and biological functions of the Amazon region, the interactions of those functions with the overall Earth system, and the impacts of changing land use on those functions. In South America, extensive floodplains are important components of the landscape throughout the Amazon River basin as well as in the Orinoco and Paraná river basins [*Junk*, 1993]. Simulation models of water and material fluxes through riverine systems require information on inundation patterns to account for the hydrological and biogeochemical effects of floodplains [*Vörösmarty et al.*, 1997]. Data on the total area and duration of flooding are required to estimate methane emissions from floodplains, which occur largely during the inundation phase, and South American floodplains are a significant source of atmospheric methane on a global scale [*Bartlett and Harriss*, 1993; *Sahagian and Melack*, 1998]. Knowledge of the spatial and temporal variability of inundation in floodplains is fundamental for the conservation and management of floodplain rivers [*Junk*, 1997; *Hamilton*, 1999]. Therefore information on inundation patterns in South American floodplains is an integral part of the data requirements for the LBA program.

[6] Inundation patterns in the major floodplains of South America have remained poorly known because of the vast size and remoteness of these areas and the difficulty of using optical remote sensing technologies such as Landsat in humid regions, where cloud cover limits the ability to acquire multiple images over time. Satellite-borne active radar systems are capable of providing spatially detailed synoptic views of geomorphology and vegetation in floodplain landscapes [*Hess and Melack*, 1994; *Hess et al.*, 1995], but the temporal coverage by processed radar imagery over the vast floodplains of South America has so far been limited to seasonal mosaics, and hence information on hydrological dynamics has been limited.

[7] Like radar, passive microwave remote sensing from satellites can reveal the presence of surface water despite cloud cover, but offers the advantage of higher temporal frequency of the available data and more years of data collection. The spatial resolution of passive microwave observations depends on the frequency of measured emission, but is coarse compared to radar. Methods have been developed to estimate flooded area from the 37-GHz polarization difference observed by the Scanning Multichannel Microwave Radiometer (SMMR), operated on board the Nimbus-7 satellite from December 1978 through August 1987. The SMMR observation period coincides with a relatively complete set of stage observations for South American rivers, and that facilitates comparison of the satellite information with ground observations of the timing of flooding. Previous publications have described the methods in detail and presented results for the fringing floodplains of the central Amazon River system and four of its major tributaries [*Sippel et al.*, 1994, 1998], the Pantanal wetland in Brazil [*Hamilton et al.*, 1996; *Hamilton*, 1999], and the Llanos de Moxos in Bolivia and Llanos del Orinoco of Venezuela and Colombia [*Hamilton et al.*, in press]. Technical issues associated with the geolocational and radiometric accuracy of the SMMR observations as well as the algorithm development for estimation of inundation area and uncertainties in the estimation are addressed in those previous publications (particularly *Hamilton et al.* [1996] and *Sippel et al.* [1998]).

Figure 1. Map of South America showing the locations of the six floodplain regions considered in this study.

[8] The present study employs the SMMR passive microwave observations in a comparative analysis of inundation patterns among six major floodplains of South America (Figure 1): 1) mainstem Amazon River floodplain in Brazil; 2) Llanos de Moxos in Bolivia; 3) Bananal Island on the Araguaía River in Brazil; 4) Llanos del Orinoco of Venezuela and Colombia; 5) savannas of Roraima State in Brazil and the adjacent Rupununi River of Guyana; and 6) Pantanal wetland, located mostly in Brazil with smaller areas in Bolivia and Paraguay. Data from previous publications on four of these regions are combined with new analyses employing similar approaches to determine inundation patterns in the Bananal and Roraima floodplains. This study provides an unprecedented comparative view of inundation patterns because the satellite observations coincide in time and were analyzed with consistent methodology.

2. Study Sites

[9] The locations of the six floodplain regions analyzed in this study are depicted in Figure 1, with additional

Table 1. Characteristics of the Grid-Cell Aggregates for Each Floodplain Region[a]

Floodplain Region	Number of Grid Cells	Number of Subregions	ΔT_{nf}	ΔT_f	Northwest Latitude, Longitude	Southeast Latitude, Longitude
Amazon mainstem	227	12	4.2	9–35	2°S, 70°W	5°S, 52°W
Llanos de Moxos	204	5	4.2	21.3–32.4	12°S, 68°W	16°S, 61°W
Bananal	119	3	4.2	33.1	9°S, 52°W	15°S, 49.5°W
Llanos del Orinoco	219	5	4.2–6.2	23.3–29.3	10°N, 72°W	4°N, 66°W
Roraima	58	1	6.1[b]	24.7	4.5°N, 61.5°W	2.25°N, 59°W
Pantanal	180	10	4.2	17–51	16°S, 58°W	21°S, 55°W

[a]The table shows the number of grid cells that were aggregated to encompass the region, the number of subregions for which the calculations were carried out, the empirically determined mean values of ΔT_{nf} and ΔT_f (in kelvins; see text for explanation), and the latitude and longitude coordinates defining rectangles that approximately encompass the grid-cell aggregates. The area of a grid cell varies slightly with latitude but is ~765 km^2.

[b]ΔT_{nf} of 6.1 K was used for Roraima unless the 2-month "precipitation excess" (see text) equaled zero, at which time no inundation of the floodplain was assumed.

information in Table 1. All of these floodplains lie at low elevations (<250 m) where the climate is tropical and humid, although the precipitation is seasonal. Together these floodplain regions comprise much of the total floodplain area in the continent. In addition, however, there is significant floodplain area along the major tributaries in the Amazon River system [*Sippel et al.*, 1992], along the upper Amazon River mainstem in Peru, along the middle and lower reaches of the Paraná River in Argentina, and in the coastal deltas of the Orinoco, Amazon, and Paraná rivers [*Junk*, 1993]. The total area of floodplains along smaller river systems is also likely to be significant [*Junk*, 1993], but has yet to be quantified.

[10] The data presented for the Amazon River floodplain represent the floodplain fringing the main stem within Brazil (known as the Solimões and Amazonas rivers), extending from the western Brazilian border (70°W) to the mouth. Tributary floodplains are not included except in the immediate vicinity of confluences. The Amazon River floodplain is largely covered with evergreen forest although more open grasslands become abundant below Santarém [*Mertes et al.*, 1995; *Junk*, 1997]. The seasonal cycle of river discharge is attenuated by the differential timing of runoff from Andean watersheds as well as lowland watersheds on both sides of the equator [*Sioli*, 1984]. The mean annual discharge of the Amazon River at Óbidos is 162,000 m^3/s [*Richey et al.*, 1989] and the annual fluctuation in stage is 7–10 m. Mean annual precipitation varies across the Amazon Basin, averaging ca. 2300 mm [*Vörösmarty et al.*, 1996]. Details on methods and results for analysis of passive microwave observations of the mainstem Amazon floodplain as well as four of its tributaries can be found in the work of *Sippel et al.* [1998].

[11] The Llanos de Moxos (also spelled as Mojos) is a savanna region located in the upper Madeira River watershed in northeastern Bolivia, mostly between the Beni, Mamoré, and Guaporé (or Iténez) rivers. In this region, the natural vegetation tends to be evergreen forest in areas that are not subject to seasonal inundation, and inundation tends to maintain grassland or savanna vegetation [*Langstroth*, 1996]. The Beni and Mamoré rivers drain montane watersheds of the Andes and carry mean annual discharges of 9000 and 8400 m^3/s, respectively, while the Guaporé River drains lower elevations to the east in Bolivia and Brazil and carries a mean annual discharge of 2100 m^3/s [*Guyot and Wasson*, 1994]. River discharge is strongly seasonal and results in large fluctuations in water level, reaching 11 m in the Mamoré River channel, although the river channels are incised into the plains and the depth of inundation in most of the savanna areas remains <1 m [*Hanagarth*, 1993]. Mean annual precipitation varies from 1300 to 2000 mm across the region, occurring mostly between September and May [*Hanagarth*, 1993]. Details on methods and results for analysis of passive microwave observations of the Moxos region can be found in the work of *Hamilton et al.* [in press].

[12] The Bananal floodplain is located in east-central Brazil along the Araguaía River, a tributary of the Tocantins River. Much of this floodplain is on the Bananal Island, which lies between two anabranches of the Araguaía River, but there is also extensive contiguous floodplain upriver of the island to 15°S latitude. The Araguaía River carries a mean annual discharge of 1680 m^3/s. The floodplain vegetation is largely savanna [*Eiten*, 1985], while surrounding uplands tend to be covered by tropical moist forest to the north and west and savanna (much converted to agriculture) to the south and east. Annual rainfall averages 1700 mm and is strongly seasonal. The Araguaía River stage varies by about 5 m over the seasonal cycle, but most of the floodplain is inundated to only 1–2 m depth or less [*Eiten*, 1985].

[13] The Llanos del Orinoco is a region of alluvial plains between the Orinoco River and the Andean foothills. The climate here tends to support savanna vegetation regardless of whether seasonal inundation occurs [*Sarmiento*, 1983], but in this study the Llanos del Orinoco region is defined as the lower-lying savanna areas that are subject to seasonal inundation. The floodplains of this region are drained by two major tributaries of the Orinoco River, both of which originate in the Andes: the Apure River (mean annual discharge, 2300 m^3/s) and the Meta River (5600 m^3/s) [*Lewis et al.*, 1995]. The Orinoco mainstem fluctuates by 10–15 m over the annual cycle, but tributary stage fluctuations are lesser within the Llanos where the floodplains absorb the excess discharge. Mean annual precipitation in the region is about 1500 mm and is strongly seasonal. Details on methods and results for analysis of passive microwave observations of the Llanos del Orinoco can be found in the work of *Hamilton et al.* [in press].

[14] The floodplains of Roraima include the savanna areas of Roraima State in northern Brazil as well as the contiguous Rupununi savannas of Guyana. Most of this territory lies within the watershed of the upper Branco River, a tributary of the Negro River that carries a mean annual discharge of 2900 m^3/s at the outflow from the region. The Rupununi savannas lie in the watershed of the Rupununi River, a smaller river that flows north into the

Essequibo River. As in the Llanos de Moxos, the presence of savanna in this region tends to indicate seasonal inundation while areas without seasonal inundation tend to be evergreen forest, although human activities may have increased the extent of grassland at the expense of forest. Floodplain vegetation includes nearly treeless grasslands as well as Mauritia palm swamps [*Beard*, 1953; *Sarmiento*, 1983]. Much of the savanna floodplain is associated with several smaller tributary rivers that have distinct upland watersheds, including the Surumu and Parime rivers. The seasonal fluctuations in stage of these tributary rivers are unknown; the Branco River at Boa Vista varies by about 6 m over the annual cycle. Rainfall averages about 1700 mm and is highly seasonal, with a marked dry season.

[15] The Pantanal wetland is located on the upper Paraguay River, mostly in Brazil with smaller areas in Bolivia and Paraguay. The Pantanal is a complex of river floodplains lying in a vast sedimentary basin filled by the deposition of alluvial fans from several tributaries. Inundation patterns in the region vary depending on the source of floodwaters (e.g., overbank flow from rivers vs. delayed drainage of precipitation) as well as backwater effects due to the limited capacity of the river channels to convey the seasonal floodwaters [*Hamilton*, 1999]. The Paraguay River drains the region and flows south to the Paraná River; in the southern Pantanal the river carries a mean annual discharge of ca. 2500 m^3/s and fluctuates in stage by about 5 m. The Pantanal supports a variety of savanna and emergent marsh vegetation; upland areas that are not subject to inundation are generally savanna vegetation although much has recently been converted to agriculture. Environments of the Pantanal are described in the works of *Junk and da Silva* [1995], *Por* [1995], and *Heckman* [1998]. Annual rainfall is 1000–1500 mm and is seasonal. Details on the methods and results for analysis of passive microwave observations of the Pantanal can be found in the work of *Hamilton et al.* [1996].

3. Methods

3.1. SMMR Data Characteristics

[16] The SMMR instrument measured the natural emission of microwave energy from the Earth's surface and atmosphere. Measurements are expressed as brightness temperatures (in Kelvins), and are available at several frequencies and at both vertical and horizontal polarizations [*Fu et al.*, 1988]. The difference between vertically and horizontally polarized brightness temperatures observed by satellite at the 37 GHz frequency (hereafter referred to as ΔT_{obs}) provides a sensitive indicator of the presence of surface water, particularly where water occurs against a background of vegetated land surfaces. *Choudhury* [1989] reviewed the theoretical basis for interpretation of 37-GHz emission. The spatial resolution of the SMMR sensor is approximately 27 km at 37 GHz and the processed global data set is gridded into cells of 0.25° latitude by longitude.

[17] Satellite observations of 37-GHz emission are available for December 1978 to August 1987 from the SMMR instrument operated on board the Nimbus-7 satellite [*Gloersen et al.*, 1984; *Fu et al.*, 1988]. This study uses the monthly SMMR observations originally described by *Choudhury* [1989, 1991]. Global SMMR observations are available for approximately 6-day intervals, and are compiled separately for day and night (local equator crossings at noon and midnight). After calculation of ΔT_{obs} for each grid cell from the daytime brightness temperatures, the observations were ranked within each month and the second lowest value (out of 4 or 5) was selected, thereby yielding one ΔT_{obs} value per month [*Choudhury*, 1989]. This screening served to eliminate outlying values that might have resulted from atmospheric scattering by heavy rainfall, or from temporary pooling of water on the land surface after heavy rainfalls.

3.2. General Approach

[18] The approximate boundaries of the floodplains were delineated using maps, remote sensing, and scientific publications, and by examination of the SMMR data for evidence of inundation. In the Llanos de Moxos, Llanos del Orinoco, and Pantanal, the subregions correspond approximately with hydrogeomorphic provinces (Table 1), although the subregion boundaries are dictated by the coarse resolution of the SMMR data. The boundaries were altered in some cases to avoid crossing or bordering major open-water features such as the largest floodplain lakes or river channels. In the cases of the Amazon and Bananal floodplains, subregions reflect arbitrary subdivisions along the direction of river flow, and the Roraima floodplains were analyzed as a single region because of their relatively small extent. Regional and subregional boundaries were chosen to encompass the floodplain subject to inundation and therefore include some upland area along the outer edges.

[19] Our general approach to determine inundation area from the SMMR ΔT_{obs} has been described in detail in the works of *Hamilton et al.* [1996] and *Sippel et al.* [1998] and will only be briefly summarized, with additional site-specific details provided for the new data that are presented. The fractional inundation area within an aggregate of SMMR grid cells was estimated using linear mixing models that account for the microwave emission of the major landscape units, or end-members, within the subregion [*Sippel et al.*, 1994]. The model has three end-members that represent the contributions of water, nonflooded land, and inundated floodplain to the ΔT_{obs}:

$$\Delta T_{obs} = f_w(\Delta T_w) + f_{nf}(\Delta T_{\mathrm{nf}}) + f_f(\Delta T_{\mathrm{f}}) \quad (1)$$

$$1 = f_w + f_{nf} + f_f \quad (2)$$

where ΔT_{obs} is the ΔT observed by the radiometer, f_w, f_{nf} and f_f are the fractional areas of open water (rivers and lakes without emergent vegetation), nonflooded land, and seasonally flooded land, respectively, and ΔT_w, ΔT_{nf}, and ΔT_{f} are the ΔT values for open water, nonflooded land, and seasonally flooded land. Simultaneous solution of equations (1) and (2) yields the following equation for the fraction of inundated floodplain (f_f):

$$f_f = \frac{\Delta T_{obs} - f_w(\Delta T_w) - \Delta T_{\mathrm{nf}} + f_w(\Delta T_{\mathrm{nf}})}{\Delta T_{\mathrm{f}} - \Delta T_{\mathrm{nf}}} \quad (3)$$

The fractional area of open water is assumed to vary little over the annual cycle, and is measured from maps or remote

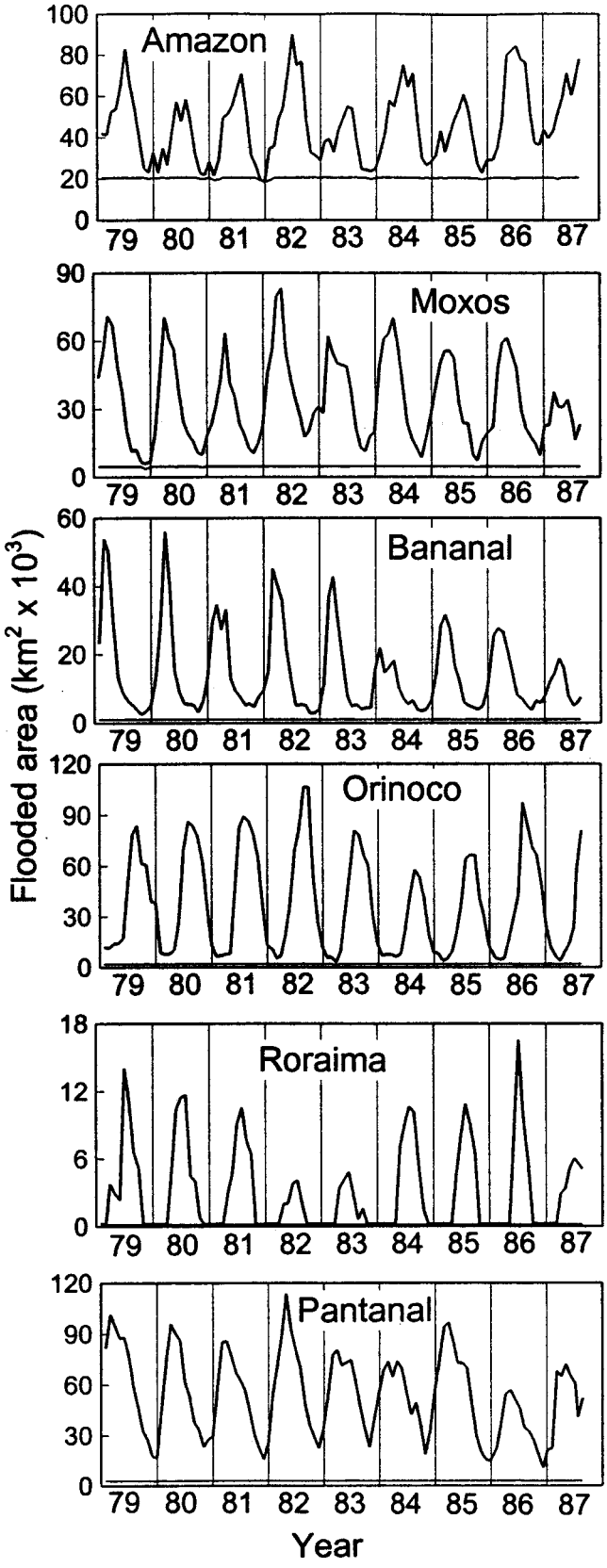

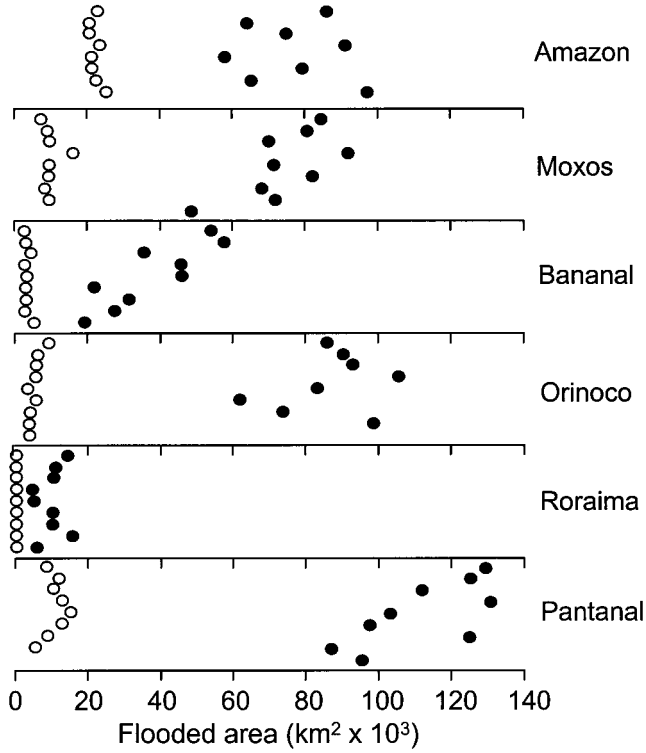

Figure 3. Distribution of annual minima and maxima of flooded area in the six floodplain regions. The annual maxima represent the total area subject to inundation in at least one month of the calendar year.

sensing imagery. The fractional area of flooded land expands during inundation with a concomitant reduction in the fractional area of nonflooded land, which includes nonflooded floodplain as well as any upland area within the grid-cell aggregate. The ΔT values for end-members in these models, which are summarized in Table 1, were determined as follows.

[20] The ΔT_{nf} values for nonflooded land were determined empirically by examination of the ΔT_{obs} measured over floodplain areas in the driest periods, as well as examination of ΔT_{obs} measured over upland areas with comparable vegetation cover. The ΔT_w value for open water cannot be determined empirically in most of these floodplain regions because the fractional coverage by open water is small, but this value is not expected to vary for calm water surfaces. In most cases a theoretical value of 60 K was used [*Choudhury*, 1989]; the ΔT_w value was determined empirically only in the Amazon floodplain

Figure 2. (opposite) Monthly estimates of total flooded area (inundated floodplain plus open water of rivers and lakes) in each of the six floodplain regions, derived from SMMR satellite observations of passive microwave emission. The dashed lines show the area of open water, which is assumed to change little throughout the year. Previous publications present these data in greater detail for the Amazon [*Sippel et al.*, 1998], the Moxos and Orinoco [*Hamilton et al.*, in press], and the Pantanal [*Hamilton et al.*, 1996].

Table 2. Summary Statistics of the Inundation Area Estimates (km^2) for the Six Floodplain Regions During the Period of SMMR Observations (1979–1987)[a]

Characteristic	Amazon	Moxos	Bananal	Orinoco	Roraima	Pantanal
Open-water area (rivers and lakes)	20,750	4,780	1,050	2,080	187	3,120
Maximum area simultaneously flooded	90,300	83,230	56,055	106,600	16,530	109,590
Maximum area subject to flooding in a calendar year	97,360	92,090	58,550	107,530	16,530	130,920
Mean flooded area, 1979–87	46,190	33,500	14,475	37,100	3,095	52,710
Long-term mean flooded area as estimated from stage records (time period)	46,920 (1903–2000)	29,460 (1967–1997)	13,110 (1974–1998)	34,700 (1927–1985)	3,480 (1967–1996)	34,880 (1900–1999)
Floodplain hydroperiod (days per year)	91	113	57	117	49	172

[a]The open-water area of rivers and lakes is included in the flooded areas. The maximum simultaneously flooded area is the maximum observed in the monthly time series of total flooded area for the region, whereas the maximum area subject to flooding is the sum of the maximum areas attained in each subregion (or individual grid cell, in the case of the Pantanal). The area subject to flooding tends to be larger because of temporal differences in flooding across the regions; for Roraima, it is the same as the maximum area simultaneously flooded because the analysis was done as a single region. The floodplain hydroperiod is defined here as the frequency at which the floodplain was inundated to $\geq$50% of its maximum inundation area over 9 years of observations; permanent open-water areas of rivers and lakes were subtracted from the floodplain area to determine hydroperiod.

where the fractional coverage by open water is large enough to do so [*Sippel et al.*, 1998].

[21] The ΔT_f values for flooded land were determined empirically for each region (except Roraima; see below) because they are expected to vary, primarily as a function of the density and structure of vegetation canopies overlying the water. Within a region, the ΔT_f could be expected to vary over the seasonal cycle of water level change, but variability in the proportion of water surface overlain by plant canopies is reduced because tree canopies generally remain emergent during inundation and herbaceous aquatic vegetation is generally composed of floating mats that rise and fall with the water level. The empirical determination was done at maximum inundation, representing the approximate midpoint of the inundation cycle. All available sources of information were considered to select calibration cells in each subregion, which are SMMR grid cells that are entirely subject to inundation in most years and can be used to determine the ΔT_f value under conditions of complete inundation [*Sippel et al.*, 1994]. The ΔT_f values from the calibration cells were averaged to yield a single estimate of ΔT_f unless there was a discernible spatial pattern in their variation.

[22] The fractional inundation area was calculated for each monthly ΔT_{obs} observation using equation (3), and inundation areas of the subregions were summed to yield the total inundation area for the region. Inundation area includes the permanent open-water area of river channels and floodplain lakes unless noted. Concurrent data on river levels (stage) from sites with long records were examined to produce predictive relationships between river stage and flooded area for each region. Mean monthly stage was computed, and cross-correlation analyses between the time series of stage and flooded area served to check for time lags of one month or more. Polynomial regression analysis yielded predictive equations to extend the inundation record over the period of river stage observations; such nonlinear predictive equations must not be employed outside of the range of stage data from which they were established.

3.3. Site-Specific Methods for Bananal and Roraima

[23] The analysis of passive microwave observations for the Bananal and Roraima floodplains has not been reported previously. Unless noted, the methods for these two floodplains are similar to those detailed for the Moxos and Orinoco floodplains in the work of *Hamilton et al.* [in press].

[24] The grid-cell aggregates for the Bananal floodplain were delineated by including all contiguous grid cells that had a standard deviation $\geq$1.5 K during the 9 years of ΔT_{obs} observations. The Bananal region extends between 9°15′ and 15°S latitude along the Araguaía River. In the Roraima region, some grid cells to the north and west of the savanna region showed elevated standard deviations for ΔT_{obs} that suggested seasonal flooding of forested wetlands. The grid-cell aggregate was confined to the contiguous savannas of the region, as depicted in the work of *Sarmiento* [1983]. The boundaries for both regions were then confirmed by comparison with independent sources of information: 1) the floodplain maps produced from Side-Looking Airborne Radar by the RADAMBrasil project and reproduced in the work of *Junk* [1993], 2) 1:250,000-scale topographic maps produced by the Brazilian government, 3) low-water Landsat images, 4) JERS radar mosaics from the National Space Development Agency of Japan, and 5) an image depicting the Normalized Difference Vegetation Index derived from the NOAA Advanced Very High Resolution Radiometer. The Bananal floodplains were arbitrarily subdivided into three subregions along the north-south axis because of a time lag in the passage of the flood peak from south to north; the divisions were made at 11°15′ and 13°15′S latitudes. The less extensive Roraima floodplains were analyzed as a single region.

[25] The permanent open-water area of river channels and lakes was measured from classified Landsat images. The river channels in these dry-season images showed areas of

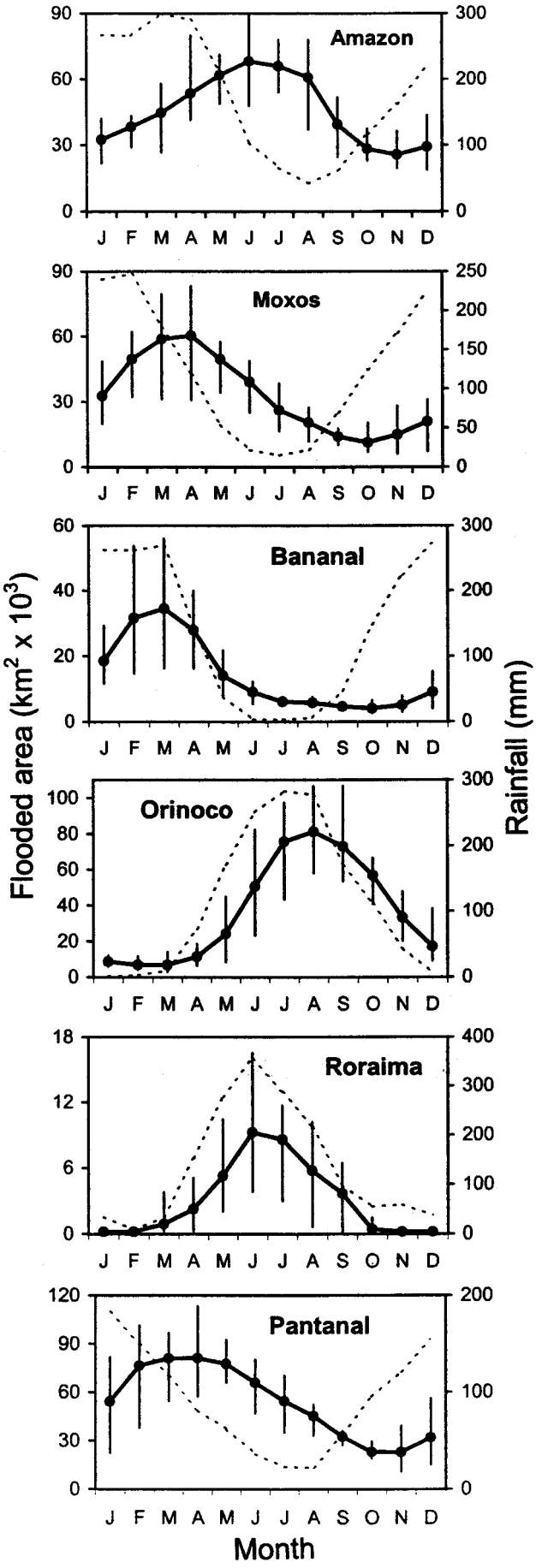

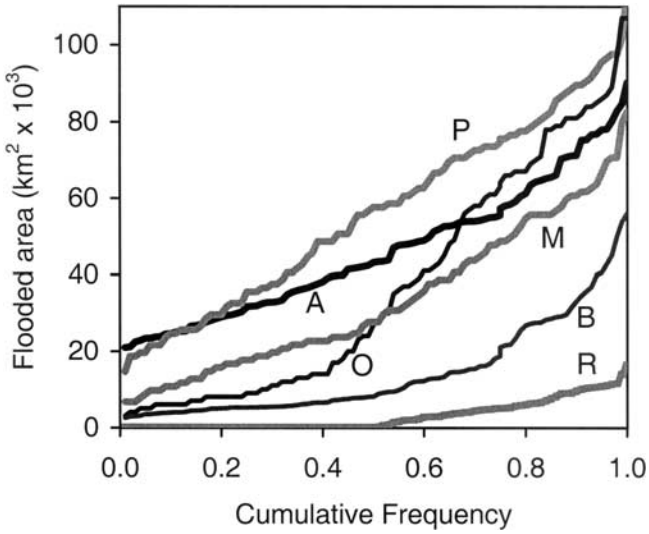

Figure 5. Flood duration curves for the six floodplain regions. Open-water area of river channels and lakes is included in the total flooded area. A = Amazon; M = Moxos; B = Bananal; O = Orinoco; R = Roraima; P = Pantanal.

sandbars that were not classified as open water, and thus open water at higher river stages may be larger. However, the fractional open-water area is not large in the Bananal and Roraima regions (Table 1) and therefore this is not important source of error in our analysis. Floodplain lakes are numerous in these regions but they tend to be very small, and hence there is little open water area outside of the river channels in these two floodplain regions.

[26] In previous work in the central Amazon floodplain and in the Pantanal region, upland areas covered by savanna or forest vegetation were observed to have a mean ΔT_{nf} of ca. 4.2 ± 1.0 K (mean ± s.d.) throughout the year [*Sippel et al.*, 1994; *Hamilton et al.*, 1996, in press]. This is close to the value expected as a result of attenuation of the microwave emission by vegetation canopies that completely cover the soil [*Choudhury*, 1989]. Examination of dry-season ΔT_{obs} values as well as information on vegetation coverage during the dry season indicate that 4.2 K is the appropriate ΔT_{nf} for the Llanos de Moxos and Bananal floodplains. However, in nonflooded savanna regions where soils are exposed among vegetation, *Justice et al.* [1989] noted slightly elevated ΔT_{obs} values, probably because the attenuating effect of the vegetation on emission from underlying soils is reduced. This phenomenon does appear to occur in the Llanos del Orinoco, where a significant increase in the ΔT_{obs} during the course of the dry season was observed in some upland and

Figure 4. (opposite) Mean monthly flooded area in the six floodplain regions over the period of satellite observations (solid line) and mean monthly rainfall based on long-term records (dashed line). Monthly means of flooded area were calculated from the data in Figure 2, and include the open-water area (rivers and permanent lakes). Vertical bars indicate the range of the monthly area estimates. Rainfall data are for the closest station with long-term records (for the Amazon floodplain, which spans a range of rainfall regimes, rain data are from near Manaus).

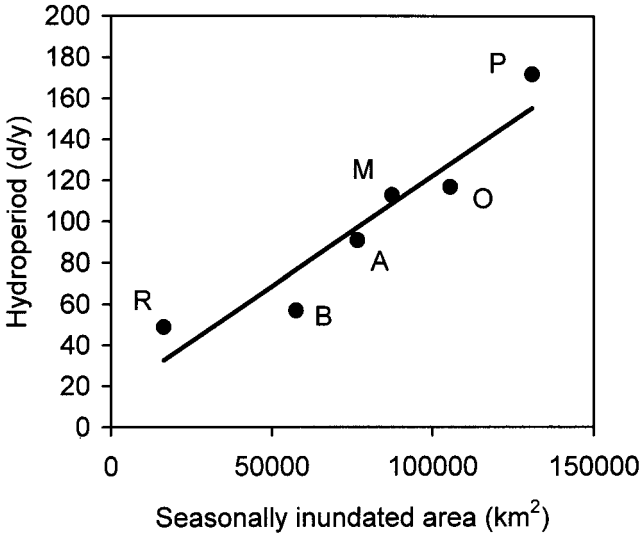

Figure 6. Relationship between hydroperiod (mean number of days per year of ≥50% inundation of the floodplain) and floodplain size. For the six regions, regression of hydroperiod (Y, in d/y) on the maximum area subject to seasonally flooding (X, in km^2) yields the following equation to predict hydroperiod from floodplain size: $Y = 0.00107X + 15.0$ ($R^2 = 0.89$, P = 0.005). The hydroperiods and maximum inundation areas shown here are for the seasonally flooded land; permanent open-water area is not included. A = Amazon; M = Moxos; B = Bananal; O = Orinoco; R = Roraima; P = Pantanal.

floodplain savannas. This increase was most likely due to increasing exposure of sand and lateritic crusts as the vegetation became sparser, and hence the ΔT_{nf} increased over time [*Hamilton et al.*, in press].

[27] As in the Orinoco, a dry-season increase in ΔT_{nf} is apparent in the Roraima region, where there was a tendency for the ΔT_{obs} to increase over the course of the dry season from about 6–7 K to 7–8 K. This increase could not be explained by flooding because monthly rainfall totals for the two stations in the region show no significant excess over the likely rate of evapotranspiration, and the river stage remained low during the dry season. The presence of exposed sandy and stony surfaces as well as the severity of the dry season have been noted in the literature on the Roraima savannas [*Beard*, 1953; *Sarmiento*, 1983], and a dry-season decrease in grassland vegetation canopies could increase the exposure of underlying soils, increasing the ΔT_{obs}. Therefore for calculation of inundation area, it was assumed that there was no inundation outside of open-water areas during month t whenever there was a "precipitation deficit" that lasted for two months, as defined by a mean monthly rainfall for months t and t-1 below 120 mm, which is a conservative estimate of monthly evapotranspiration in the region [*Hills*, 1968; *Salati*, 1985]. Rainfall data are means for two rainfall measurement stations, one at Boa Vista (2°49′47″N, 60°39′42″W) and the other at Fazenda Passarão (3°12′28″N, 60°34′16″W). A ΔT_{nf} = 6.1 K was used for the calculation of fractional inundation area on the remainder of the dates, which was the mean ΔT_{obs} value observed early in the dry seasons, corrected for the permanent open-water contribution.

[28] The ΔT_f value for Bananal was determined empirically from a set of 12 calibration cells, as was done previously for the other floodplains. The relatively small Roraima region does not have large homogeneous expanses of floodplain that fill entire grid cells, and thus the ΔT_f could not be determined empirically there. Therefore the algorithms for Roraima employ the mean ΔT_f value for 39 calibration cells in the 4 subregions of the Llanos del Orinoco that most closely resemble the savannas of Roraima (excluding the more deeply flooded Apure Delta subregion).

[29] Relationships between mean monthly river stage or rainfall and flooded area were evaluated using the closest river stage or rainfall stations that had long records. Stage and rainfall data were obtained from the Brazilian Agência Nacional de Energia Elétrica (ANEEL). For the Bananal floodplain, there was a good correlation between flooded area and the Araguaía River stage at Luiz Alves (13°12′35″S, 50°35′6″W). For the Roraima floodplain, there was a good correlation between flooded area and the stage of the Branco River at Boa Vista (2°49′47″N, 60°39′42″W), which is located downriver of most of the floodplain. Compared to river stage, rainfall was not as well correlated with floodplain inundation area in either floodplain region.

4. Results and Discussion

4.1. Passive Microwave Observations of Inundation Area

[30] Time series of the total flooded area in each of the regions show considerable variability in the total extent of inundation in these floodplains, both seasonally as well as interannually (Figure 2). This variability is easier to visualize as a dot plot depicting the distribution of the annual minima and maxima (Figure 3). The maximum extent of inundation is variable among years in all of these floodplains, with the greatest relative variation in Bananal and Roraima. In most cases nearly all of the land that was subject to seasonal inundation became dry each year. The Pantanal appears to retain the most flooded area at low water, but this is due to the long time lag (4–6 months) for passage of the flood across the region; most individual subregions become largely dry in most years [*Hamilton et al.*, 1996].

[31] In floodplains where there are time lags for the passage of the flood across the region, the total area of land subject to inundation is larger than the maximum area of simultaneous inundation. Table 2 shows both the maximum area that was simultaneously flooded and the max-

Figure 7. (opposite) Relationships between flooded area derived from passive microwave remote sensing and ground observations of river stage in each of the six floodplain regions. Table 3 contains details on the stage sites and regression models.

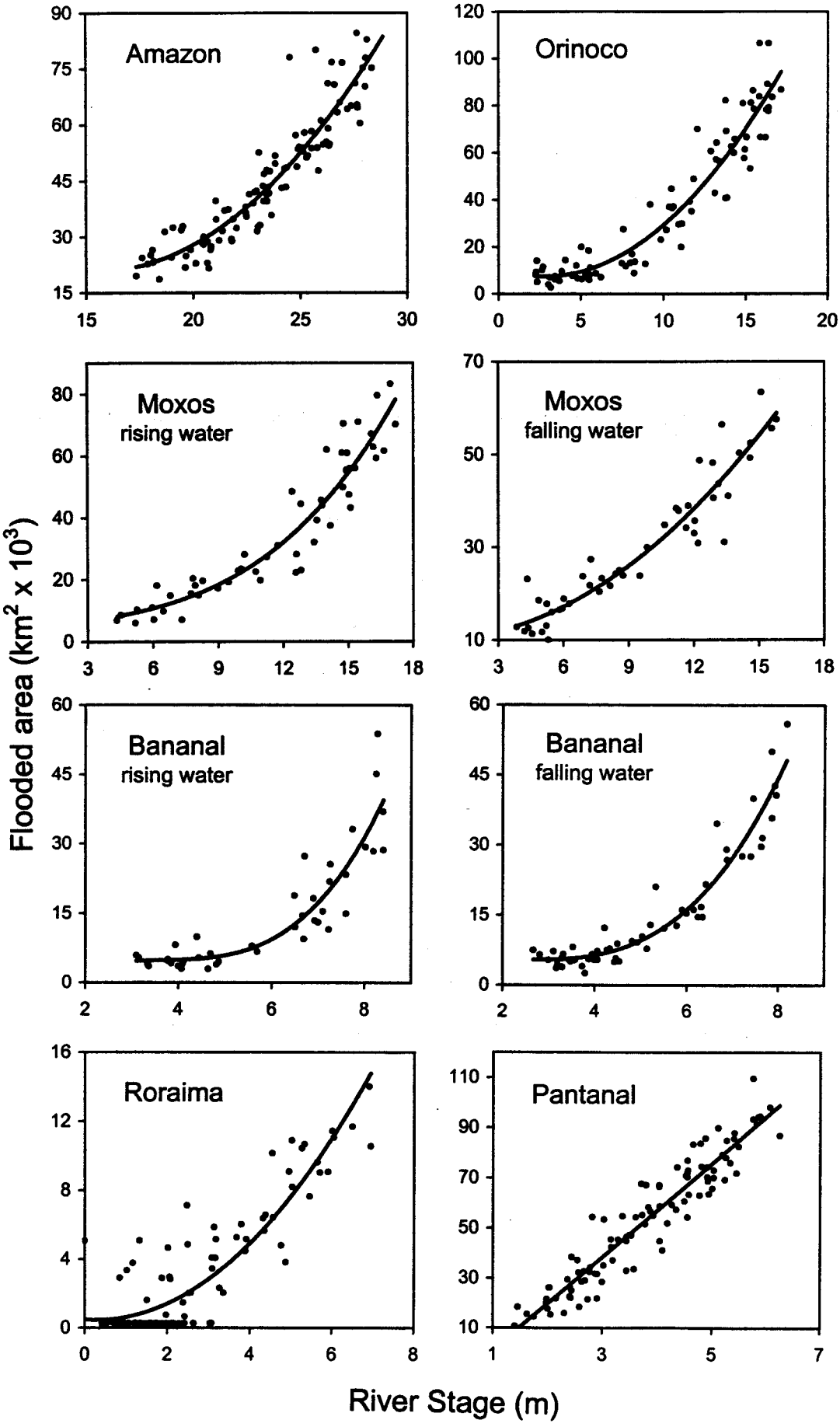
Amazon
Orinoco
Moxos
rising water
Moxos
falling water
Bananal
rising water
Bananal
falling water
Roraima
Pantanal
Flooded area (km^2 x 10^3)
River Stage (m)

Table 3. Empirical Relationships to Predict Flooded Area From River Stage[a]

Floodplain Region (No. of Data Pairs)	River Stage Station (River Name)	Range of Stage (1979–1987), m	Lag months	Regression Equations				
				R^2	A	B	C	D
Amazon mainstem (102 dates)	Manaus (Negro River)	17.3–28.9	0	0.87	104,744	−10,851	351	–
Llanos de Moxos: rising stage (54)	Porto Velho (Madeira)	4.3–17.2	0	0.90	3,139	1,296.1	−104.04	16.423
Llanos de Moxos: falling stage (48)	Porto Velho (Madeira)	3.9–15.8	0	0.90	9,916	51.109	193.06	–
Bananal: rising stage (42)	Luiz Alves (Araguaía)	3.1–8.4	0	0.83	13650	139.78	−0.36308	3.2348×10^{-4}
Bananal: falling stage (58)	Luiz Alves (Araguaía)	2.7–8.2	0	0.92	5792	15.707	−0.11138	1.9026×10^{-4}
Llanos del Orinoco (84):	Ciudad Bolívar (Orinoco)	2.3–17.2	0	0.90	10784	−2388.5	423.34	–
Roraima (102)	Boa Vista (Branco)	0.4–7.0	1	0.81	−164.52	217.70	271.92	–
Pantanal (102)	Ladário (Paraguay)	1.3–6.4	1.5[b]	0.90	−17,309	18,520	–	–

[a]Flooded area includes open water area of lakes and rivers. These equations are derived from the data in Figure 7 and can be employed to extend the inundation record over the period of stage observations, provided that the stage remains within the range of the 1979–1987 period. The coefficients of determination (R^2) provide an indication of the degree to which water levels in the major rivers associated with these floodplains reflect the extent of seasonal inundation. Time lags were incorporated when they improved the prediction; for example, a lag of 1 month means that the predictive relationship employed the mean river stage from the following month to predict mean flooded area in a particular month. The regressions of inundated area (Y, in km^2) on stage (X, in m) take the form of $Y = A + BX + CX^2 + DX^3$.

[b]For the Pantanal, the regression uses the mean stage of the following 2 months because of the long time delay for passage of the flood across the region and the downstream location of the stage station [*Hamilton et al.*, 1996].

imum area subject to flooding in at least one month of the calendar year. Using the latter area as a definition of floodplain extent, the Pantanal is the largest floodplain (130,920 km^2), followed by the Llanos del Orinoco (107,530 km^2). Roraima is the smallest of the floodplains analyzed, and is the only region that appears to dry completely for several months each year (except for river channels and small permanent floodplain lakes).

[32] The timing of flooding and drainage also varies among the four regions, as depicted by the mean flood hydrographs (Figure 4). The variable timing of inundation reflects the local wet and dry seasons, which are different on either side of the equator. The Amazon River receives its discharge from subbasins on both sides of the equator, resulting in a less marked seasonal cycle. Comparison of the mean seasonal cycles of rainfall and inundation shows how each region except for Roraima has a time lag of variable duration between rainfall in the watershed and flooding on the floodplains. The Amazon, Llanos de Moxos, and Pantanal tend to reach peak inundation 2–3 months after the height to the local wet season and retain substantial flooding during the local dry season, while flooding of the Bananal, Llanos del Orinoco, and Roraima floodplains is more synchronous with the local wet season. Perhaps the most dramatic example among the six floodplain regions is the Pantanal, where inundation in the southernmost subregions can occur at the peak of the local dry season, producing a verdant floodplain when adjacent upland soils are dry, grasslands are brown, and many trees have shed their leaves. As the flood waters recede the rains tend to increase and terrestrial vegetation thrives, in contrast to floodplains such as Roraima where the rainy season is nearly synchronous with floodplain inundation and the dry season is a time of limited water availability in much of the floodplain.

[33] Flood duration curves shown in Figure 5 reveal characteristic patterns for each floodplain and can be used to estimate exceedance frequencies, as is commonly done with river discharge. One way to consider the duration of floodplain inundation (or floodplain hydroperiod) is to use the flood duration curves to determine the frequency at which the floodplain was inundated to $\geq$50% of its maximum inundation area over the 9 years of observations, and to express this frequency as the average number of days per year (Table 2). The hydroperiod as defined here applies only to the seasonally inundated floodplain, and thus the permanent open-water area of rivers and lakes has been subtracted for determination of the 50% inundation exceedance frequencies. These hydroperiod estimates show considerable variation, ranging from a maximum of 172 days for the Pantanal to only 57 and 49 days for the Bananal and Roraima floodplains, respectively. The duration of the hydroperiod is positively correlated with the total area of seasonally inundated land, reflecting the tendency for more

Figure 8. (opposite) Long-term record extension based on the prediction of flooded area from river stage (equations in Table 3). Open-water area is included in the total flooded area. The duration of each record is determined by the availability of stage data. For the Amazon and Pantanal, river stage sometimes fell below the range of observations used to develop the predictive relationship; a fixed lower limit of inundation area was used on those dates to avoid extrapolation. Previous publications present these record extensions for the Amazon [*Sippel et al.*, 1998] and the Pantanal [*Hamilton et al.*, 1996], but they have been updated to 1999 in this figure.

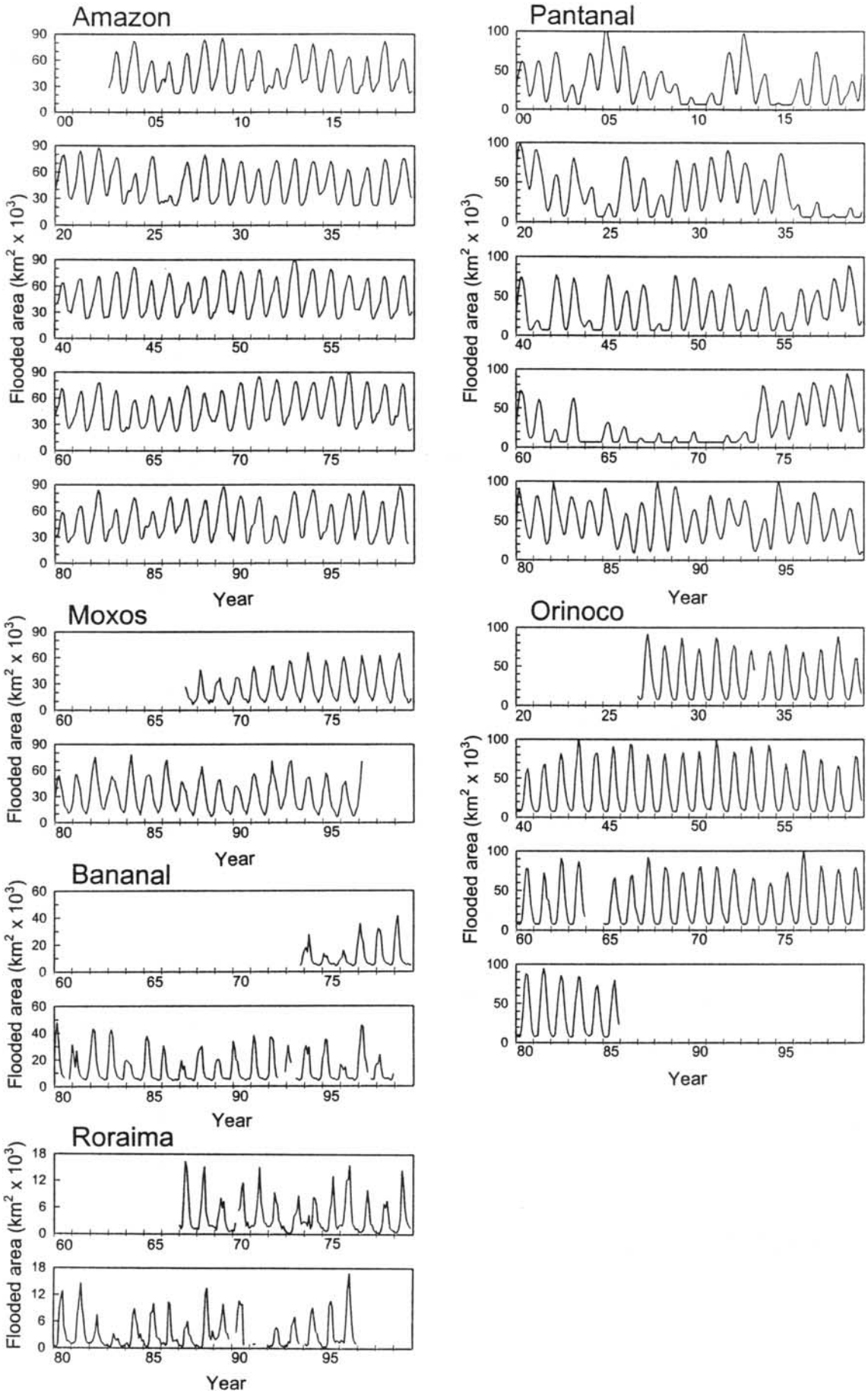
Amazon
Pantanal
Moxos
Orinoco
Bananal
Roraima
Flooded area (km² x 10³)
Year

Table 4. Means for the Maximum Annual Inundation Over the Extended Records Depicted in Figure 8[a]

Floodplain Region	Long-Term Mean (km^2) and c.v. (%) of Maximum Annual Inundation	No. of Years in Record
Amazon	73,246 (14%)	98
Llanos de Moxos	57,100 (19%)	31
Bananal	29,587 (31%)	25
Llanos del Orinoco	80,337 (12%)	58
Roraima	10,914 (35%)	29
Pantanal	59,072 (46%)	100

[a]Inundation area includes the permanent open waters of rivers and lakes (open-water areas are given in Table 1). Variability in maximum annual inundation is expressed as the coefficient of variation of the mean (c.v., in %).

protracted flooding in larger floodplains where the flow paths for drainage of floodwaters to the rivers are longer (Figure 6).

4.2. Extension of the Inundation Record

[34] The relationships between flooded area derived from passive microwave remote sensing and ground observations of river stage reveal the degree to which floodplain inundation is linked to water level in the major rivers associated with the floodplains. This information is increasingly needed to assess the environmental impact of river channel modifications, including impoundments as well as navigation projects. For example, *Hamilton* [1999] examined stage/flooded area relationships for subregions of the Pantanal to show how inundation of much of the floodplain is directly linked to water levels in the rivers. A correlation between river stage and flooded area does not necessarily imply control of flooding by the river level at that measurement station, however, as exemplified in the cases of the Moxos and Orinoco floodplains where the selected stage stations are located far downriver of the floodplain regions.

[35] Figure 7 depicts the stage/flooded area relationships and Table 3 summarizes the predictive equations to extend the inundation record over the longer time period for which river stage observations are available. The relationship between flooded area and stage tends to be nonlinear because at lower stages the rivers are confined within their banks, while at higher stages the river increasingly establish connectivity with their floodplains and flooded area increases rapidly with stage. At flood stages, the stage/flooded area relationship is determined by the floodplain geomorphology as well as time lags for filling and drainage of the more extensive floodplains. Time lags may also exist when the stage measurement station is downriver of much or all of the floodplain, as is the case for the Llanos de Moxos, Llanos del Orinoco, and the Pantanal. If the time lags are approximately one month or greater, a better relationship can be obtained by incorporating a lag into the regression, which was done for the Roraima and Pantanal floodplains. In cases where distinct relationships with flooded area were observed at rising and falling stages, separate predictive equations were employed.

[36] The extended records of inundation depicted in Figure 8 provide a better indication of interannual variability than the 9-year SMMR time series, even though the regression technique does not capture the full range of variability in maximum and minimum flooding extent [*Moog et al.*, 1999]. Long-term means for inundation area in these extended records resemble the means for the 9-year SMMR period, except for the Pantanal where the long-term mean is considerably lower (Table 3). The mean and coefficient of variation for the maximum annual inundation areas in each of the extended series are given in Table 4. A marked flood pulse occurred in the Amazon and Orinoco floodplains in nearly all years, resulting in the lowest coefficients of variation in Table 4. In contrast, the Pantanal shows the greatest interannual variability in maximum inundation, with a tendency for multi-year periods of drier or wetter conditions and some years with relatively little flooding. Occasional protracted dry periods with little flooding, as for example in the Pantanal from 1960 to 1973, strongly impact wildlife populations, produce changes in floodplain vegetation, and can result in the expansion of human activities on the floodplain. Records for the Bananal and Roraima floodplains are shorter but also show considerable variability in the magnitude of the flood pulse. The Llanos de Moxos inundation record, extending back to 1967, shows somewhat less variability in the maximum inundation. In the years 1967–1973, when the Pantanal was in the latter part of a protracted drought, the Moxos floodplains were evidently still subject to substantial flooding, albeit less than in subsequent years. The interannual variability in inundation in these regions is caused by climatic variability that is driven in part by sea surface temperature anomalies in the tropical Pacific Ocean [*Hastenrath*, 1990; *Robertson and Mechoso*, 1998].

[37] Information on the mean annual inundation area is required to estimate rates of trace gas exchange between tropical wetlands and the atmosphere. The lack of data on the mean flooded area for each of the major tropical wetlands has limited the accuracy of these estimates. For example, previous attempts to estimate methane emission rates have assumed that tropical floodplains were fully inundated for 50% of the year, which is equivalent to a mean inundation area of 50% of the total area [e.g., *Matthews and Fung*, 1987; *Bartlett and Harriss*, 1993], or they have assigned an average duration of inundation for different categories of wetlands based on site-specific studies [*Aselmann and Crutzen*, 1989]. The aforementioned studies also differ substantially in the total areas of South American wetlands used in the calculations. Comparison of the long-term mean annual inundation area to the total area subject to inundation in Table 2 shows that the mean inundation area ranges between 22–48% of the total area (five of the six range 22–32%). The higher inundation percentage for the Amazon floodplain is due to the larger fraction of permanent open waters. These results show that the assumption of 50% inundation leads to overestimation of methane emission rates by nearly two-fold in wetlands that are largely composed of seasonally inundated lands, which are the most extensive kind in South America. *Aselmann and Crutzen* [1989] assumed that "seasonal floodplains" were inundated for 3.5 months per year (equivalent to 29% mean inundation), which is quite close to the results reported here. The total floodplain areas reported here are also similar to those used by *Aselmann and Crutzen* [1989], based on information from diverse

sources that was originally compiled and eventually published by *Junk* [1993].

5. Conclusions and Future Work

[38] The SMMR observations of passive microwave emission have provided new insights into the dynamics of inundation in these vast floodplains, which is fortuitous considering that the sensor system was not designed for observation of flooding [*Choudhury*, 1989]. The fluctuations in flooded area could be characterized despite the coarse spatial resolution of the sensor system because of the large extent of these floodplains. Smaller floodplains or those with more erratic fluctuations in flooded area would be more difficult to study using the SMMR observations and would require sensor systems with greater spatial resolution as well as new ground observations for calibration and validation.

[39] Additional satellite observations of passive microwave emission have been made by the Special Sensor Microwave Imager since the SMMR deployment ended in 1987, as part of the Defense Meteorological Satellite Program [*Hollinger et al.*, 1990]. New sensor systems such as the Conical Microwave Imager Sounder [*Flaming*, 2000] should maintain continuity in the global record of passive microwave emission measurements. Correction for atmospheric interference is increasingly feasible and should reduce the variance in the measurements [*Choudhury et al.*, 1992; *Prigent et al.*, 1997, 1998]. In addition, other remote sensing approaches such as synthetic aperture radar [*Hess et al.*, 1995] and radar altimetry [*Birkett*, 1998] have begun to produce complementary information on these floodplains. Challenges that lie ahead include calibration and validation of the newer passive microwave sensor systems to yield a continuous record of comparable inundation observations, and the synergistic combination of the information on inundation patterns from passive microwave emission with data on geomorphology, vegetation, and water levels that are increasingly available from other kinds of remote sensing systems.

[40] **Acknowledgments.** This research was based upon work supported by the U.S. National Aeronautics and Space Administration under grants NAGT 30013, NAGW-2724, NAGW-4352, NCC5-281, and by the National Science Foundation under grant DEB-9701714. Numerous local and international scientists assisted with our research and contributed to our comprehension of these floodplain regions, but we especially wish to acknowledge the support of the staff of the Pantanal research center operated by the Empresa Brasileira de Pesquisa AgropecuÃria. We also acknowledge the AgÕncia Nacional de Energia ElÕtrica, the Brazilian Navy, and the firm Hidrologia SA for the Brazilian stage and rainfall data, and the Venezuelan Ministerio del Ambiente y de los Recursos Naturales Renovables for the Orinoco River stage data. This research was greatly enhanced by the efforts of anonymous citizens and government employees who faithfully maintained river stage observations over many decades. D. Skole and W. Chomentowski of the Basic Science Remote Sensing Initiative at Michigan State University (a NASA Earth System Information Partner) provided the Landsat imagery and assistance with its analysis, D. Moog offered statistical advice, E. M. M. Novo assisted with the Amazon work, and L. Hess provided JERS radar mosaics and commented on the manuscript. This is contribution 962 of the W. K. Kellogg Biological Station.

References

Aselmann, I., and P. J. Crutzen, Global distribution of natural freshwater wetlands and rice paddies, their net primary productivity, seasonality and possible methane emissions, *J. Atmos. Chem.*, *8*, 307–358, 1989.

Bartlett, K. B., and R. C. Harriss, Review and assessment of methane emissions from wetlands, *Chemosphere*, *26*, 261–320, 1993.

Beard, J. S., The savanna vegetation of northern tropical America, *Ecol. Monogr.*, *23*, 149–215, 1953.

Birkett, C. M., Contribution of the TOPEX NASA radar altimeter to the global monitoring of large rivers and wetlands, *Water Resour. Res.*, *34*, 1223–1239, 1998.

Choudhury, B. J., Monitoring global land surface using Nimbus-7 37 GHz data, theory and examples, *Int. J. Remote Sens.*, *10*, 1579–1605, 1989.

Choudhury, B. J., Passive microwave remote sensing contribution to hydrological variables, *Surv. Geophys.*, *12*, 63–84, 1991.

Choudhury, B. J., E. R. Major, E. A. Smith, and F. Becker, Atmospheric effects on SMMR and AAM/I 37 GHz polarization difference over the Sahel, *Int. J. Remote Sens.*, *13*, 3443–3463, 1992.

Eiten, G., Vegetation near Santa Teresinha, NE Mato Grosso, *Acta Amazonica*, *15*, 275–301, 1985.

Flaming, M., The conical microwave imager sounder, *Earth Observer*, *12*, 18–21, 2000.

Fu, C. C., D. Han, S. T. Kim, and P. Gloersen, *User's Guide for the Nimbus 7 Scanning Multichannel Microwave Radiometer (SMMR) CELL-ALL Tape*, Ref. Publ. 1210, U.S. National Aeronautics and Space Administration, Washington, D.C., 1988.

Gloersen, P., et al., A summary of results from the first Nimbus 7 SMMR observations, *J. Geophys. Res.*, *89*, 5335–5344, 1984.

Guyot, J. L., and J. G. Wasson, Regional pattern of riverine dissolved organic carbon in the Amazon drainage basin of Bolivia, *Limnol. Oceanogr.*, *39*, 452–458, 1994.

Hamilton, S. K., Potential effects of a major navigation project (the Paraguay–Paraná Hidrovía) on inundation in the Pantanal floodplains, *Reg. Rivers Res. Manage.*, *15*, 289–299, 1999.

Hamilton, S. K., S. J. Sippel, and J. M. Melack, Inundation patterns in the Pantanal wetland of South America determined from passive microwave remote sensing, *Arch. Hydrobiol.*, *137*, 1–23, 1996.

Hamilton, S. K., S. J. Sippel, D. F. Calheiros, and J. M. Melack, An anoxic event and other biogeochemical effects of the Pantanal wetland on the Paraguay River, *Limnol. Oceanogr.*, *42*, 257–272, 1997.

Hamilton, S. K., S. J. Sippel, and J. M. Melack, Seasonal inundation patterns in two large savanna floodplains of South America: The Llanos de Moxos (Bolivia) and the Llanos del Orinoco (Venezuela and Colombia), *Hydrol. Processes*, in press.

Hanagarth, W., *Acerca de la geoecología de las sabanas del Beni en el noreste de Bolivia*, 186 pp., Instituto de Ecología, La Paz, Bolivia, 1993.

Hastenrath, S., Diagnostics and prediction of anomalous river discharge in northern South America, *J. Clim.*, *3*, 1080–1096, 1990.

Heckman, C. W., *The Pantanal of Poconé: Biota and ecology of the northern section of the world's largest pristine wetland*, *Monographiae Biologicae*, vol. 77, 592 pp., Kluwer Acad., Norwell, Mass., 1998.

Hess, L. L., and J. M. Melack, Mapping wetland hydrology and vegetation with synthetic aperture radar, *Int. J. Ecol. Environ. Sci.*, *20*, 197–205, 1994.

Hess, L. L., J. M. Melack, S. Filoso, and Y. Wang, Delineation of inundated area and vegetation along the Amazon floodplain with the SIR-C synthetic aperture radar, *IEEE Trans. Geosci. Remote Sens.*, *33*, 896–904, 1995.

Hills, T. L., *Climatic Observations, No. 5, St. Ignatius, Rupununi District, Guyana*, Savanna Res. Proj. Ser., Department of Geography, McGill University, Montreal, 1968.

Hollinger, J. P., J. L. Pierce, and G. A. Poe, SSM/I instrument evaluation, *IEEE Trans. Geosci. Remote Sens.*, *28*, 781–790, 1990.

Junk, W. J., Wetlands of tropical South America, in *Wetlands of the World: Inventory, Ecology and Management*, vol. I, edited by D. F. Whigham, D. Dykyjová, and S. Hejný, pp. 679–739, Kluwer Acad., Norwell, Mass., 1993.

Junk, W. J., (Ed.), The central amazon floodplain: Ecology of a pulsing system, *Ecological Studies*, vol. 126, Springer-Verlag, New York, 1997.

Junk, W. J., and C. J. da Silva, Neotropical floodplains: A comparison between the Pantanal of Mato Grosso and the large Amazonian River floodplains, in *Limnology in Brazil*, edited by J. G. Tundisi, C. E. M. Bicudo, and T. M. Tundisi, pp. 195–217, Brazilian Academy of Sciences and Brazilian Limnological Society, Rio de Janeiro, 1995.

Junk, W. J., P. B. Bayley, and R. E. Sparks, The flood-pulse concept in river–floodplain systems, in *Proceedings of the International Large River Symposium*, edited by D. P. Dodge, pp. 110–127, Can. Spec. Publ. Fish. Aquat. Sci. 106, National Research Council of Canada, Ottawa, Ontario, 1989.

Junk, W. J., J. J. Ohly, M. T. F. Piedade, and M. G. M. Soares (Eds.), *The Central Amazon Floodplain: Actual Use and Options for a Sustainable Management*, Backhuys Publishers, Leiden, Netherlands, 2000.

Justice, C. O., J. R. G. Townshend, and B. J. Choudhury, Comparison of

AVHRR and SMMR data for monitoring vegetation phenology on a continental scale, *Int. J. Remote Sens.*, *10*, 1607–1632, 1989.

Langstroth, R. P., *Forest islands in an Amazonian savanna of northeastern Bolivia*, Ph.D. thesis, Department of Geography, University of Wisconsin-Madison, 1996.

Lewis, W. M., Jr., and J. F. Saunders III, Concentration and transport of dissolved and suspended substances in the Orinoco River, *Biogeochemistry*, *7*, 203–240, 1989.

Lewis, W. M., Jr., S. K. Hamilton, and J. F. Saunders III, Rivers of northern South America, in *Ecosystems of the World: Rivers*, edited by C. Cushing, G. W. Minshall, and K. Cummins, pp. 219–256, Elsevier Sci., New York, 1995.

Matthews, E., and I. Fung, Methane emission from natural wetlands: Global distribution, area, and environmental characteristics of sources, *Global Biogeochem. Cycles*, *1*, 61–86, 1987.

Mertes, L. A. K., D. L. Daniel, J. M. Melack, B. Nelson, L. A. Martinelli, and B. R. Forsberg, Spatial patterns of hydrology, geomorphology, and vegetation on the floodplain of the Amazon River in Brazil from a remote sensing perspective, *Geomorphology*, *13*, 215–222, 1995.

Mertes, L. A. K., T. Dunne, and L. A. Martinelli, Channel–floodplain geomorphology along the Solimões–Amazon River, Brazil, *Geol. Soc. Am. Bull.*, *108*, 1089–1107, 1996.

Moog, D. B., P. J. Whiting, and R. B. Thomas, Streamflow record extension using power transformations and application to sediment transport, *Water Resour. Res.*, *35*, 243–254, 1999.

Por, F. D., *The Pantanal of Mato Grosso (Brazil): World's Largest Wetlands*, 122 pp., Kluwer Acad., Norwell, Mass., 1995.

Prigent, C., W. B. Rossow, and E. Matthews, Microwave land surface emissivities estimated from SSM/I observations, *J. Geophys. Res.*, *102*, 21,867–21,890, 1997.

Prigent, C., W. B. Rossow, and E. Matthews, Global maps of microwave land surface emissivities: Potential for land surface characterization, *Radio Sci.*, *33*, 745–751, 1998.

Richey, J. E., L. A. K. Mertes, T. Dunne, R. L. Victoria, B. R. Forsberg, C. Tancredi, and E. Oliveira, Sources and routing of the Amazon River flood wave, *Global Biogeochem. Cycles*, *3*, 191–204, 1989.

Robertson, A. W., and C. R. Mechoso, Interannual and decadal cycles in river flows of southeastern South America, *J. Clim.*, *11*, 2570–2581, 1998.

Sahagian, D., and J. M. Melack (Eds.), Global wetland distribution and functional characterization: trace gases and the hydrologic cycle, Int. Geosphere Biosphere Program Rep. 46, 92 pp., International Geosphere Biosphere Program Secretariat, Stockholm, 1998.

Salati, E., The climatology and hydrology of Amazonia, in *Amazonia*, edited by G. T. Prance and T. E. Lovejoy, pp. 18–48, Pergamon, New York, 1985.

Sarmiento, G., The savannas of tropical America, in *Tropical Savannas*, edited by F. Bourliere, pp. 245–288, *Ecosystems of the World*, vol. 13, Elsevier Sci., New York, 1983.

Sioli, H., The Amazon and its main affluents: Hydrography, morphology of the river courses, and river types, in *The Amazon: Limnology and Landscape Ecology of a Mighty Tropical River and Its Basin*, edited by H. Sioli, pp. 127–166, Dr. W. Junk Publishers, Dordrecht, 1984.

Sippel, S. J., S. K. Hamilton, and J. M. Melack, Inundation area and morphometry of lakes on the Amazon River floodplain, Brazil, *Arch. Hydrobiol.*, *123*, 385–400, 1992.

Sippel, S. J., S. K. Hamilton, J. M. Melack, and B. J. Choudhury, Determination of inundation area in the Amazon River floodplain using the SMMR 37 GHz polarization difference, *Remote Sens. Environ.*, *48*, 70–76, 1994.

Sippel, S. J., S. K. Hamilton, J. M. Melack, and E. M. M. Novo, Passive microwave observations of inundation area and the area/stage relation in the Amazon River floodplain, *Int. J. Remote Sens.*, *19*, 3055–3074, 1998.

Vörösmarty, C. J., C. J. Willmott, B. J. Choudhury, A. L. Schloss, T. K. Stearns, S. M. Robeson, and T. J. Dorman, Analyzing the discharge regime of a large tropical river through remote sensing, ground-based climatic data, and modeling, *Water Resour. Res.*, *32*, 3137–3150, 1996.

Vörösmarty, C. J., R. Wasson, and J. E. Richey, Modeling the transport and transformation of terrestrial materials to freshwater and coastal ecosystems, Int. Geosphere Biosphere Program Rep. 39, 84 pp., International Geosphere Biosphere Program Secretariat, Stockholm, 1997.

Welcomme, R. L., River fisheries, FAO Fisheries Tech. Pap. 262, 330 pp., Food and Agriculture Organization of the United Nations, Rome, 1985.

Wilcox, R., Cattle and environment in the Pantanal of Mato Grosso, Brazil, 1870–1970, *Agric. Hist.*, *66*, 232–256, 1992.

S. K. Hamilton (corresponding author) and S. J. Sippel, W. K. Kellogg Biological Station and Department of Zoology, Michigan State University, 3700 East Gull Lake Drive, Hickory Corners, MI 49060-9516, USA. (hamilton@kbs.msu.edu)

J. M. Melack, Institute for Computational Earth System Science and Department of Ecology, Evolution, and Marine Biology, University of California, Santa Barbara, CA 93106-3060, USA.